66. Hills, J. G. *Nature* **311**, 636–638 (1984).
67. Wetherill, G. W. *Bull. Am. astr. Soc.* **18**, 763 (1986).
68. Shoemaker, E. M. & Wolfe, R. F. in *The Galaxy and the Solar System* (eds Smoluchowski, R., Bahcall, J. N. & Matthews, M.) 338–386 (Univ. Arizona Press, Tucson, 1986).
69. Glass, B. P., R. Swincki, M. B. & Zwart, P. A. *Proc. lunar planet. Sci. Conf.* **10**, 2535 (1979).
70. Storzer, D. & Wagner, G. A. *Naturwissenschaften* **67**, 90–91 (1980).
71. Storzer, D., Jessberger, E. K., Klay, N. & Wagner, G. A. *Meteorites* **19**, 317 (1984).
72. Glass, B. P. *Earth planet. Sci. Lett.* (submitted).
73. Flessa, K. W. & Jablonski, D. *Paleobiology* **9**, 315–321 (1983).
74. Berggren, W. A., Kent, D. V. & Flynn, J. J. *Geol. Soc. Lond. spec. Pap.* (in the press).
75. Montanari, A. *et al. Geology* **13**, 596–599 (1985).
76. Prinn, R. G. *Eos* **66**, 813 (1985).
77. Lewis, Z. S., Watkins, G. H., Hartman, H. & Prinn, R. G. *Spec. Pap. geol. Soc. Am.* **190**, 215–221 (1982).
78. Hansen, T. A. *Palaios* (in the press).
79. Birkeland, T. & Bromley, R. G. (eds) *Cretacious–Tertiary Boundary Events: Symposium 1, The Maastrichtian and Danian of Denmark* (Univ. Copenhagen, 1979).
80. Christensen, W. K. & Birkeland, T. (eds) *Cretacious–Tertiary Boundary Events: Symposium 2, Proceedings* (Univ. Copenhagen, 1979).
81. Mount, J. F., Margolis, S. V., Showers, W., Ward, P. & Doehne, E. *Palaios* **1**, 87–92 (1986).
82. Hansen, T. A., Farrand, R., Montgomery, H. & Billman, H. in *The Cretaceous–Tertiary Boundary and Lower Tertiary of the Brazos River Valley* (ed. Yancey, T. E.) 21–36 (Am. Assn. Pet. Geol., Texas, 1984).
83. Mabesoone, J. M., Tinoco, I. M. & Coutinho, P. N. *Palaeogeogr. Palaeoclimatol. Palaeoecol.* **4**, 161–185 (1968).
84. Kauffman, E. G. & Johnson, C. C. *Science* (submitted)
85. Kauffman, E. G. & Sohl, N. F. *Verh. Naturf. Ges. Basel* **84**, 399–467 (1974).
86. Liebau, A. *Proc. Colloq. Eur. Micropalaeont.* **13**, 3–28 (1973).
87. Liebau, A. *Neues Jb. Geol. Palaeone*, **157**, 233–237 (1978).
88. Wiedmann, J. *Estud. Geol.* **20**, 107–148 (1964).
89. Ward, P., Wiedmann, J. & Mount, J. F. *Geology* **14**, 899–903 (1986).
90. Heinberg, C. in *Cretaceous–Tertiary Boundary Events: Symposium 1, The Maastrichtian and Danian of Denmark* (eds Birkelund, T. & Bromley, R. G.) 58 (Univ. Copenhagen, 1979).
91. Birkelund, T. in *Cretaceous–Tertiary Boundary Events: Symposium 1, The Maastrichtian and Danian of Denmark* (eds Birkelund, T. & Bromley, R. G.) 51–57 (Univ. Copenhagen, 1979).
92. Smit, J. *Spec. Pap. geol. Soc. Am.* **190**, 329–352 (1982).
93. Perch-Nielsen, K., McKenzie, J., Quziang, H. *Spec. Pap. geol. Soc. Am.* **190**, 353–371 (1982).
94. Thierstein, H. *Spec. Pap. geol. Soc. Am.* **190**, 385–399 (1982).
95. Thierstein, H. *Spec. Publs. Soc. econ. Paleont. Miner.* **32**, 355–394 (1981).
96. Thierstein, H. R. & Okada, H. in *Init. Rep. DSDP* **43**, 601–616 (1979).
97. Herm, D. *Deutsche Geol. Ges. Zeitschur. Jahrg.* **15**, 277–348 (1963).
98. Surlyk, F. & Johannsen, M. D. *Science* **233**, 1174–1177 (1984).
99. Birkelund, T. & Hakansson, E. *Spec. Pap. geol. Soc. Am.* **190**, 373–384 (1982).
100. Boersma, A. & Shackleton, N. J. *Init. Rep. DSDP* **62**, 513–526 (1981).
101. Smit, J. & van der Kaars, S. *Science* **223**, 1177–1179 (1984).
102. Arthur, M. A. & Schlanger, S. O. *Bull. Am. Ass. Petrol. Geol.* **63**, 870–885 (1979).
103. Elder, W. P. in *Fine-Grained Deposits and Biofacies of the Cretaceous Western Interior Seaway: Evidence of Cyclic Sedimentary Processes* (eds Pratt, L. M., Kauffman, E. G. & Zelt, F. B.) 157–169 (Soc. Econ. Paleontol. Mineralog., Tulsa, 1985).
104. Elder, W. P. thesis, Univ. Colorado (1987).
105. Kauffman, E. G. in *Treatise on Invertebrate Paleontology*, Pt A (eds Robinson, R. A. & Teichert, C.) 418 (Geol. Soc. Am., Univ. Kansas Press, 1978).
106. Pratt, L. M. in *Fine-Grained Deposits and Biofacies of the Cretaceous Western Interior Seaway: Evidence of Cyclic Sedimentary Processes* (eds Pratt, L. M., Kauffman, E. G. & Zelt, F. B.) 38 (Soc. Econ. Paleontol. Mineralog., Tulsa, 1985).
107. Kauffman, E. G. *Geol. Ass. Can. spec. Pap.* **27**, 273–306 (1984).
108. Kauffman, E. G. *Geol. Soc. Am. Abstr. Progm.* **16**, 555 (1984).
109. Kauffman, E. G. & Hansen, T. *Eos* **66**, 46; 813 (1985).
110. Grieve, R. A. F. *Spec. Pap. geol. Soc. Am.* **190**, 25–37 (1982).
111. Leckie, R. M. in *Fine-Grained Deposits and Biofacies of the Cretaceous Western Interior Seaway: Evidence of Cyclic Sedimentary Processes;* (eds Pratt, L. M., Kauffman, E. G. & Zelt, F. B.) 139–150 (Soc. Econ. Paleontol. Mineralog., Tulsa, 1985).
112. Eicher, D. L. & Diner, R. in *Fine-Grained Deposits and Biofacies of the Cretaceous Western Interior Seaway: Evidence of Cyclic Sedimentary Processes* (eds Pratt, L. M., Kauffman, E. G. & Zelt, F. B.) 60–71 (Soc. Econ. Paleontol. Mineralog., Tulsa, 1985).
113. Koch, C. F. thesis, George Washington Univ. (1977).
114. Koch, C. F. *Paleobiology* **6**, 184–192 (1980).
115. Cobban, W. A. & Scott, G. R. *Prof. Pap. U.S. geol. Surv.* **645**, 108 (1972).
116. Birkelund, T. *et al. Bull. geol. Soc. Danm.* **33**, 1–108 (1984).
117. Watkins, D. K. in *Fine-Grained Deposits and Biofacies of the Cretaceous Western Interior Seaway: Evidence of Cyclic Sedimentary Processes* (eds Pratt, L. M., Kaufmann, E. G. & Zelt, F. B.) 151–156 (Soc. Econ. Paleontol. Mineralog., Tulsa, 1985).
118. Gentner, W., Kirsten, T., Storzer, D. & Wagner, G. A. *Earth planet. Sci. Lett.* **20**, 204–210 (1973).
119. McDougall, I. & Lovering, J. F. *Geochim. cosmochim. Acta* **33**, 1057–1070 (1969).
120. Storzer, D. & Wagner, G. A. *Meteoritics* **14**, 541–542 (1979).
121. Storzer, D. & Wagner, G. A. *Meteoritics* **12**, 368–369 (1977).
122. Storzer, D. *Meteoritics* **20**, 765–766 (1985).
123. Cobban, W. A. in *Fine-grained Deposits and Biofacies of the Cretaceous Western Interior Seaway: Evidence of Cyclic Sedimentary Processes* (eds Pratt, L. M., Kauffman, E. G. & Zelt, F. B.) 135–138 (Soc. Econ. Paleontol. Mineralog., Tulsa, 1985).

ARTICLES

Stratospheric trace gases in the spring 1986 Antarctic atmosphere

C. B. Farmer, G. C. Toon, P. W. Schaper, J.-F. Blavier & L. L. Lowes

Jet Propulsion Laboratory, California Institute of Technology, Pasadena, California 91109, USA

The atmospheric absorption features of over 500 infrared solar spectra recorded at McMurdo Station, have been analysed to determine the vertical column abundances of trace gases crucial to the understanding of the 'ozone hole' phenomenon.

SATELLITE measurements[1,2] have now established that the springtime ozone depletion, first reported by Farman *et al.*[3], extends throughout the polar vortex, a region of the atmosphere isolated by the polar circulation during the Antarctic winter and usually centred over eastern Antarctica. During September and October 1986, a period during which we monitored the atmosphere above McMurdo Station (78° S, 166° E), we were fortunate that we were near the centre of the ozone hole on two occasions; 15–22 September and 15–23 October. The edge of the hole, as defined by the maximum ozone gradient, was close to McMurdo on three occasions: 5–8 September, 23–28 September and 6–13 October. Thus, our observations sampled the polar atmosphere deep inside the vortex as well as the warmer regions close to the edge.

The observations were made with the JPL MkIV Interferometer, a high-resolution Michelson interferometer built specifically for recording atmospheric spectra from remote ground-based sites, aircraft and from stratospheric balloons. The instrument is double-passed with one fixed and one moving corner reflector, allowing a 200-cm maximum optical path difference. For the majority of the spectra recorded at McMurdo the maximum path difference of the scans was limited to 66 cm, giving an unapodized spectral resolution of 0.01 cm^{-1}. The carriage which holds the moving reflector is driven by a flexible integrating nut riding on a lead screw. This arrangement, together with the double-passed optical scheme, makes the instrument resistant to the effects of mechanical distortion and shock; this was especially important when operating under the conditions of wind and thermal stress encountered in the Antarctic environment. The spectral range of the instrument is covered by two detectors: an InSb detector is used for the shorter wavelengths (1.8–5.5 μm, 1,800–5,500 cm^{-1}) and a HgCdTe photoconductor for the range 5.5–15 μm (650–1,800 cm^{-1}). Both detectors are cooled to liquid nitrogen temperatures. The optical path difference between the two arms of the interferometer is monitored during the scan by a He–Ne laser whose interference fringes are used to trigger the sampling of the two signal channels. At the sampling rate of 10^4 s^{-1}, each pair of one million-point interferograms is recorded in 100 s.

An advantage of this technique is that the measurements of all of the constituents are made simultaneously in the same airmass, so that the results presented here represent self-contained inventories for each day. Due to the low solar angles, the stratospheric airmass sampled by our instrument was, at times, as much as 200 km away from the observation site, a point to remember when comparisons are made between these and other measurements made in slightly different airmasses.

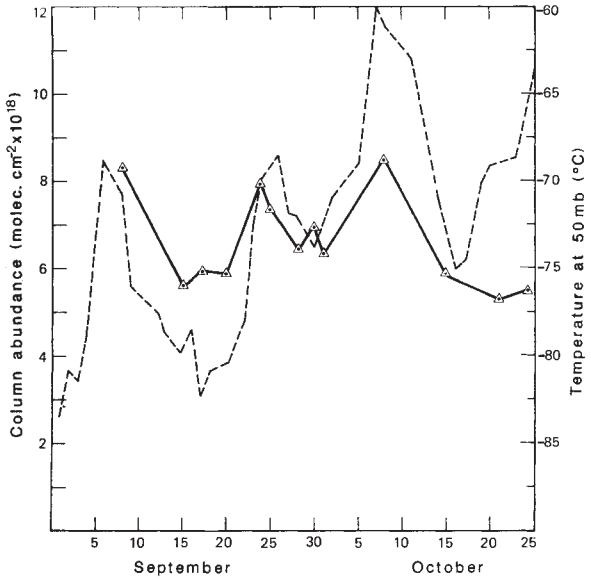

Fig. 1 Vertical column abundances of ozone over McMurdo Station during September and October, 1986. The dotted line shows the temperature at the 50-mb level.

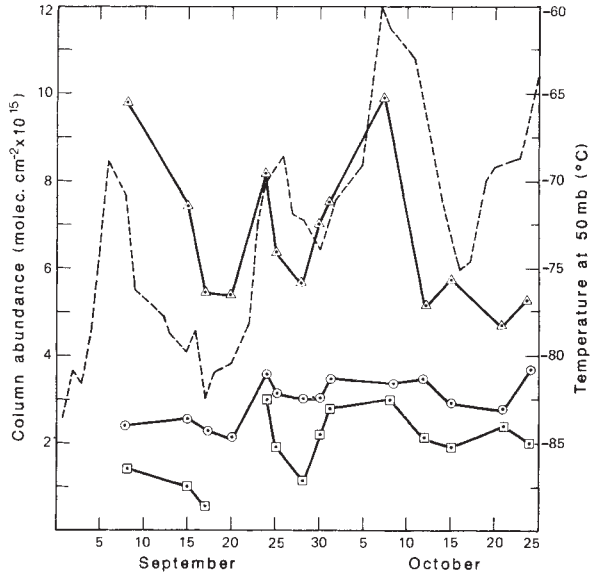

Fig. 2 As Fig. 1, for HNO_3 (△), NO (○) and NO_2 (□). Note that the HNO_3 values are shown at half scale.

Data from 14 days have been analysed to examine the variations of the column abundances of several related gases whose behaviour should provide clues for discriminating between the different mechanisms that have been suggested to explain the ozone hole. Table 1 lists the values of the solar zenith and azimuth angles for the beginning and end of the observation periods during which the spectra were recorded. The results for the stratospheric trace gases are summarized in Table 2 and in Figs 1, 2 and 3. The short-term variations (on a timescale of days) are a reflection of the movement of the polar vortex; the longer-term changes reveal the variations of stratospheric composition in the vortex that accompany the ozone depletion. In common with other studies, we have chosen the temperature at the 50-mb level as the characteristic parameter to describe the sampled airmass and against which to examine correlations of the column abundances of the related trace constituents. These temperatures were collated from radiosonde measurements made at McMurdo by the United States Navy and by the University of Wyoming (D. Hoffman, personal communication) during our observing period, and are superimposed on Figs 1, 2 and 3 showing the time variation of the constituent abundances.

The analysis of the spectra was performed by scaling an assumed volume mixing ratio profile for a particular molecule until the spectrum calculated using this profile best matched the measured spectrum over a small wavenumber interval, or 'microwindow', in which the spectral lines of the molecule are free from blending with lines of other gases. Table 3 lists the microwindows used for the molecules reported here. The temperature and pressure profiles used in the calculation were interpolated from the radiosonde measurements of Hoffman *et al.*[4]; as these radiosonde flights were made about twice per week, the potentially large temperature error on some days dictated our choice of temperature-insensitive spectral lines whenever possible.

The retrieval of a vertical column abundance from an atmospheric absorption feature requires knowledge of both the volume mixing ratio profile of the gas and the trajectory of the solar radiation through the atmosphere. The latter was established by numerical tracing of a ray backwards through the refracting atmosphere until it emerged at the correct astronomical solar zenith angle, computed from the known latitude, longitude, time and the solar ephemeris. The accuracy of the parameters used in this calculation becomes critical for low solar-elevation observations; but a sensitive internal check on the validity of the ray geometry assigned to each spectrum is provided by CO_2, whose line strengths and mixing ratio have been determined to

Table 1 Summary of observation periods used for the present analysis

Date	Local time* start	Solar angle (deg.) zenith	azimuth	Local time stop	Solar angle (deg.) zenith	azimuth
8 September	11.23	84.6	22.0	11.57	84.1	13.5
15 September	12.09	81.3	9.9	13.00	81.1	357.1
17 September	11.15	81.3	23.2	11.43	80.8	16.2
20 September	13.46	79.5	345.2	13.58	79.7	342.2
24 September	11.37	78.1	17.1	11.41	78.1	16.1
25 September	13.13	77.3	353.0	13.40	77.5	346.2
28 September	13.05	76.1	354.7	13.41	76.4	345.7
30 September	13.46	75.7	344.3	14.04	76.0	339.8
1 October	13.23	75.0	350.0	14.12	75.8	337.7
8 October	05.47	87.3	103.5	06.14	85.9	96.7
12 October	14.00	71.4	339.9	14.13	71.7	336.7
15 October	05.02	86.9	114.3	05.48	84.6	102.8
21 October	14.02	68.2	339.0	14.30	68.8	332.0
24 October	13.46	66.8	342.8	14.06	67.2	337.8

* Local time, GMT+12 h.

Table 2 Observed vertical column abundances (molec. cm^{-2})

Molecule	O_3† ($\times 10^{18}$)	O_3 ($\times 10^{18}$)	NO ($\times 10^{15}$)	NO_2 ($\times 10^{15}$)	HNO_3 ($\times 10^{15}$)	$ClONO_2$ ($\times 10^{15}$)	HCl ($\times 10^{15}$)
Date							
8 September	7.79	8.47 ± 0.20‡	2.4 ± 0.5	1.4 ± 0.5	19.6 ± 0.5	2.5 ± 0.5	1.56 ± 0.10
15 September	6.15	5.57 ± 0.20	2.6 ± 0.6	1.0 ± 0.4	14.9 ± 0.4	1.8 ± 0.3	1.48 ± 0.10
17 September	5.51	5.98 ± 0.15	2.3 ± 0.4	0.5 ± 0.5	10.9 ± 0.2	1.5 ± 0.2	1.58 ± 0.10
20 September	5.83	5.92 ± 0.05	2.1 ± 1.0	2.0 ± 4.0	10.8 ± 0.2	2.0 ± 0.2	2.04 ± 0.15
24 September	8.04	8.06 ± 0.20	3.6 ± 0.6	3.0 ± 2.5	16.6 ± 0.5	4.5 ± 0.4	2.69 ± 0.15
25 September	7.04	7.37 ± 0.15	3.1 ± 0.2	1.9 ± 0.4	12.7 ± 0.4	3.7 ± 0.2	2.84 ± 0.10
28 September	6.26	6.44 ± 0.10	3.0 ± 0.2	1.1 ± 0.4	11.2 ± 0.2	3.0 ± 0.2	2.85 ± 0.05
30 September	6.48	6.99 ± 0.15	3.0 ± 0.5	2.2 ± 0.5	14.1 ± 0.2	3.8 ± 0.4	2.88 ± 0.10
1 October	6.26	6.33 ± 0.12	3.5 ± 0.5	2.8 ± 0.5	15.1 ± 0.2	3.7 ± 0.2	2.99 ± 0.10
8 October	7.28	8.55 ± 0.05	3.4 ± 0.3	3.0 ± 0.2	20.0 ± 0.2	3.5 ± 0.1	4.15 ± 0.05
12 October	6.56	6.95 ± 0.05	3.5 ± 0.4	2.1 ± 0.5	10.2 ± 0.1	3.4 ± 0.5	4.20 ± 0.05
15 October	5.78	5.85 ± 0.05	2.9 ± 0.2	1.9 ± 0.3	11.5 ± 0.2	2.5 ± 0.1	4.17 ± 0.05
21 October	5.13	5.29 ± 0.60	2.8 ± 0.8	2.4 ± 0.6	9.4 ± 0.4	2.4 ± 1.2	3.65 ± 0.25
24 October	5.67	5.55 ± 0.40	3.7 ± 0.5	2.0 ± 1.5	10.7 ± 0.3	1.5 ± 0.8	5.29 ± 0.25

* HF, $1.80 \pm 0.01 \times 10^{15}$. † Latitude-corrected TOMS O_3 column values, see text. ‡ The global errors represent precisions, see text.

high accuracy elsewhere. Tests showed that for weak, temperature-independent absorption features, and solar zenith angles $\leq 85°$, the error due to the use of an incorrect volume mixing ratio profile is small. The analysis was therefore concentrated on the spectra taken at the highest elevation angles, even though these, because of their characteristically shallower absorptions, resulted in somewhat lower precision. Of the molecules discussed here, HNO_3 shows the largest dependence of the derived column abundance on the assumed vertical profile. This results from two factors: (1) the accessible spectral lines are temperature-dependent (−0.4% per °C) and (2) they are opaque at the line centres, resulting in nonlinear growth of their absorption. Numerical tests using a range of realistic vertical profiles showed that the derived HNO_3 column varies over a maximum range of ±15%. But provided the shape of the profile did not change appreciably during the observation period, errors in the assumed profile introduce a systematic bias which does not invalidate the derived day-to-day variations in the column amount.

The absolute accuracy of the molecular spectral parameters[5] used in the analysis limits the accuracies of the derived column abundances for most of the gases discussed here. The exceptions to this are NO and NO_2, which have such small absorptions that on days when the SNR is poor the accuracy of the column becomes limited by random error. The $ClONO_2$ Q-branch at 780 cm^{-1} has only recently been measured at low temperatures[6] and over an extended spectral range[7]; the results of these new measurements indicate a potential 30% error in our derived column values for $ClONO_2$. Spectral line parameters of the ν_5 band of HNO_3 used here are incomplete; Brown *et al.*[5] claim an accuracy of 10% for the integrated intensities of the four fundamental bands of HNO_3. As the microwindow used for HNO_3 includes five manifolds, each of which contains several prominent lines, we believe that 20% is an appropriate accuracy for our derived columns, although individual spectral lines may be uncertain by more than this. The O_3, HCl and HF line parameters are estimated to be accurate to 5% (ref. 5). But errors in the assumed strengths of the spectral lines enter the analysis as systematic effects so that, provided the same features are used for each spectrum analysed, only errors in the assumed temperature dependences of the line strengths and Lorentz widths coupled to actual temperature changes will affect the precision of the day-to-day variations. These temperature dependences are well known in all cases (except for $ClONO_2$) and are automatically accounted for in the analysis procedure. Therefore, as the importance of the derived column abundances lies primarily in their trends and correlations, rather than their absolute values, we feel it appropriate to quote errors corresponding to estimates of relative precision rather than absolute accuracy, so that significant day-to-day variations are still apparent. These error estimates listed in Table 2, are the standard deviations of column abundances obtained from individual spectra. It is evident from examination of the errors that the quality of the data varied considerably, chiefly because of the effects of wind buffeting the instrument on some days.

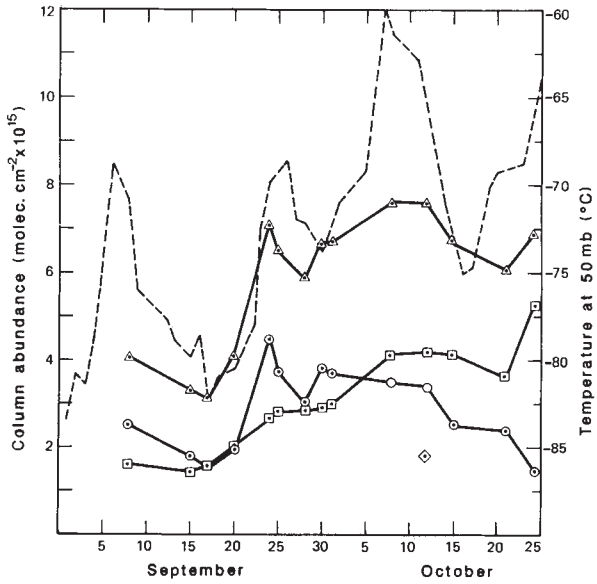

Fig. 3 As Fig. 1, for the chlorine reservoir species HCl (□), $ClONO_2$ (○) and their sum (△). The column abundance value for HF obtained on 12 October 1986 is also shown (◇).

Table 3 Principal microwindows used for analysis

Constituent	Central frequency and width (cm^{-1})
CO_2	2,632.36, 2,636.63 (0.2)
O_3	1,154.61 (0.2)
HNO_3	868.10 (2.0)
$ClONO_2$	780.25 (0.7)
NO	1,900.05, 1,903.13 (0.2)
NO_2	2,914.65 (0.1)
HCl	2,843.63, 2925.90, 2963.29 (0.1)
HF	4,038.96 (0.2)

Trace gases

Ozone. As an example of the precision attainable by this method, Fig. 4 shows measured and calculated spectra at 1,154 cm^{-1}, one

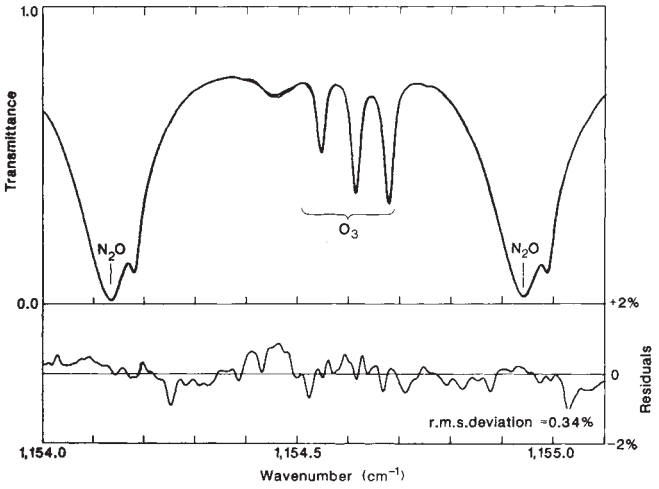

Fig. 4 Comparison of calculated and measured spectra over a region including the triplet of ozone lines at 1,154.6 cm^{-1} used to derive the O_3 column abundances. The observed data were taken on 8 October 1986 at a solar zenith angle 85.9°. The residuals (measured minus calculated) have been included to emphasize the small differences between the spectra.

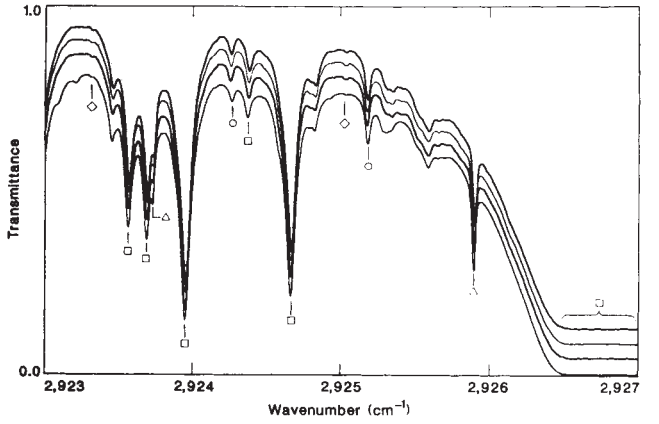

Fig. 5 Examples of a calculated spectrum (lower trace) and three consecutive measured spectra (offset for clarity) taken on 8 October 1986 at a solar zenith angle of 87.1°. These illustrate the reproducibility of the observations and the high quality of the spectral line parameters used in the calculations. Some of the more significant absorptions are identified: □, CH_4; ○, H_2O; △, HCl; ◇, NO_2.

of many ozone microwindows; the r.m.s. deviation between the calculated and measured spectra is typically 0.35% for a single scan. To validate our ozone measurements, we calculated where the path of the observed solar radiation had passed through the ozone layer and then estimated the total ozone mapping spectrometer (TOMS) O_3 column at that location from the latitudinal O_3 gradient (ref. 2 and A. J. Krueger, personal communication). When we were close to the edge of the ozone hole this gradient was as large as 10% per degree (latitude), and the corrections on these occasions were considerable. Comparison of our O_3 total column values with the latitudinally corrected TOMS values (Table 2) gives a good indication of the general agreement between the methods. The residual systematic difference of ~5% is a reflection of the accuracy of the spectral parameters used in the analysis.

Nitrogen species. It has been postulated[8] that the Antarctic ozone depletion is a natural phenomenon linked to the solar cycle, the ozone reduction being caused by enhanced levels of nitrogen oxides produced as a result of increased solar activity. Our measured NO_2 values (Fig. 2) were abnormally small, especially in mid-September when they fell below 1×10^{15} cm^{-2}. Bearing

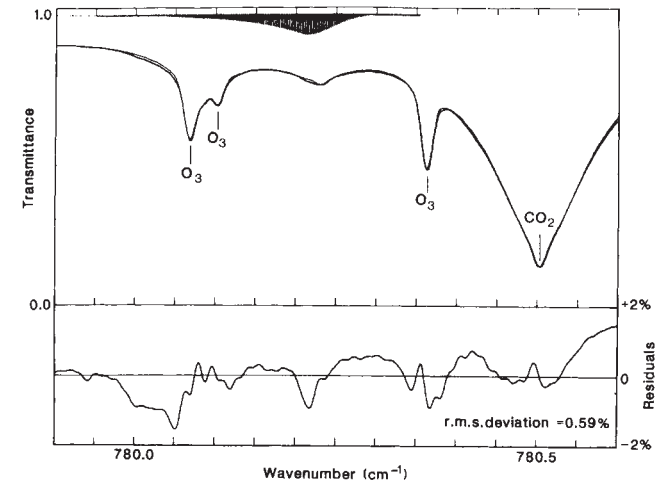

Fig. 6 Observed and computed spectra in the 780.2 cm^{-1} microwindow for $ClONO_2$, from data taken on 15 October 1986 at a solar zenith angle of 85.6°. The lower trace shows the residuals while the upper tick marks represent the positions and strengths of the $ClONO_2$ spectral lines used in the calculation.

in mind the lower altitude of the polar NO_2 layer[11], the peak volume mixing ratios were therefore greatly reduced in comparison with mid-latitudes[9,10]. NO_2 columns recovered to ~3×10^{15} cm^{-2} when the edge of the hole was close to McMurdo, but never exceeded mid-latitude values. These results agree with the visible measurements of Mount *et al.*[11] to within the error estimates. NO followed the same trends as NO_2, with the difference that the bulk of the NO which, on the basis of mid-latitude profiles, is assumed to be located above the region of the ozone depletion, moderated the fluctuations in its total column abundance. The column abundances of HNO_3, which are plotted at half-scale in Fig. 2, show large fluctuations, the maximum values being larger by a factor of two than the values obtained from measurements using the same spectral interval at lower latitudes[9,10].

Halogen sinks and reservoirs. The behaviour of the principal chlorine reservoirs, hydrochloric acid (HCl) and chlorine nitrate ($ClONO_2$), is shown in Fig. 3; examples of the spectral fits obtained in the analysis of these gases are illustrated in Figs 5 and 6. The HCl column amounts, which are derived from the analysis of several absorption lines, show an increase from an initial low value of 1.5×10^{15} cm^{-2} to 4.2×10^{15} cm^{-2} by mid-October. A further rapid increase to 5.3×10^{15} cm^{-2} occurred during the last few days of observation, an almost fourfold increase overall. The corresponding column value for the stratospheric component of HCl at mid-latitudes is 1.5×10^{15} cm^{-2} (refs 9, 12).

The $ClONO_2$ results show a similar trend (but with much larger day-to-day variations) until the beginning of October, after which there is a marked reversal and the column amounts decrease for the remainder of the period. The polar $ClONO_2$ column values are considerably higher, with respect to mid-latitude amounts[13], than the HCl values. The variation of the total amount of chlorine in the reservoirs (which is assumed to be the sum of HCl and $ClONO_2$) is also plotted in Fig. 3; this shows a very close correlation with the stratospheric temperature and an increase of a factor of two between September and October.

When discussing the sinks and reservoir species, note that the measurements themselves yield values only for the vapour phase abundances of the constituents. The increase in the chlorine reservoirs between September and October, both inside and 'outside' the hole, suggests either that substantial fractions of the HCl and $ClONO_2$ are held in some condensed form, for example, as polar stratospheric clouds, before October, or that

'missing' chlorine is present in the atmosphere in some other molecular form which we have not yet been able to identify in the spectra. The former possibility is supported, in a qualitative sense, by the correlation of the reservoir species with the stratospheric temperature. In the absence of significant condensation, however, the deficit to be made up by an alternate molecular form of chlorine is large—at least 4×10^{15} cm^{-2}—and species with even the weakest line strengths would be readily detected at the high signal-to-noise ratio of these observations, unless their absorption bands coincided with opaque regions of the spectrum; strong methane and nitrous oxide lines, for example, hamper the search for Cl_2O_2 in the 1,200 cm^{-1} region of the spectrum. Conservative estimates of the minimum column amounts of ClO which would give rise to discernible spectral features at 850 cm^{-1} in our spectra in September and October were 2×10^{1} cm^{-2} and 1×10^{15} cm^{-2}, respectively. The present results taken alone, therefore, do not preclude the possibility that relatively large amounts of ClO, but $<2\times10^{15}$ cm^{-2}, are present in the stratosphere during September and early October. The missing chlorine cannot be accounted for by ClO alone, however.

In either of the above cases, the partitioning of chlorine between $ClONO_2$ and HCl is unusual, and very different from the observed situation at lower latitudes, where measurements and model predictions are in good agreement[13]. The mid-latitude column values for $ClONO_2$ and stratospheric HCl are 7×10^{14} and 1.5×10^{15} cm^{-2}, respectively. By comparison, the corresponding values for McMurdo in October were both approximately 4×10^{15} cm^{-2}. The partitioning between the two reservoirs reverts to a ratio more typical of lower latitudes towards the end of October. It is evident that the chlorine chemistry of the Antarctic stratosphere is perturbed during the early spring season.

The sink for fluorine, hydrofluoric acid (HF), was measured on one day only, towards the end of the observing period at McMurdo, because the wavelength of the absorption band of HF lies outside the normal operating range of the instrument. The spectra that were obtained for HF were of very high quality and the derived column abundance, 1.80×10^{15} cm^{-2}, has an estimated accuracy of 5%. This measurement provides a key reference point in assessing the validity of the Antarctic halogen budget suggested by these results. Manmade chemicals are the only known source of fluorine in the atmosphere and HF in the stratosphere is the direct result of the photolysis of CFCs. The column abundance of HF at McMurdo is about three times larger than the corresponding value at mid-latitudes[9,12], presumably a consequence of the stratospheric circulation and the long lifetime of HF. The ratio HF/HCl in the upper stratosphere is important in understanding the effects of injection of halogenated chemicals as it resolves the complication that arises because chlorine has natural as well as anthropogenic sources, coupled with the fact that HCl is removed more easily than HF from the atmosphere. This ratio at mid-latitudes is presently 1/4 (ref. 9), a value which has increased from 1/10 over the ten years since its distribution was first measured[14]. From the McMurdo measurements, the fluorine to chlorine ratio for the Antarctic stratosphere was found to be close to 1/4 also, after the total chlorine (taken here as the sum of $ClONO_2$ and HCl) had reached its maximum value (by the beginning of October). This suggests that by October most of the chlorine was in the vapour phase with very little of it being in any form other than HCl or $ClONO_2$.

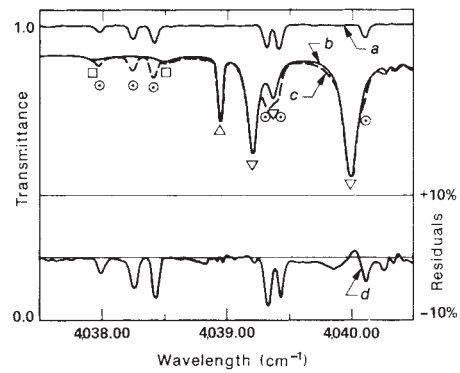

Fig. 7 The spectrum in the region of the R1 line of HF at 4,038.96 cm^{-1} is illustrated. The upper trace (*a*), taken from the solar spectrum recorded by the ATMOS instrument[15] from an altitude of 250 km, shows several absorption lines of the 2-0 band of CO in the solar photosphere. The two superimposed spectra are a single scan recorded at McMurdo at a solar zenith angle of 71.5° (*b*) and the corresponding calculated spectrum (*c*). The residual plot (*d*) shows that the large differences between the observed and calculated spectra are due to the solar lines, which are not included in the calculation, and that the HF line is isolated from any interference from either solar or telluric absorptions. ○, solar CO; □, HDO; ▽, H_2O and ◇, HF. The fit to the observed spectrum in the proximity of the HF line is better than 1%.

Conclusions

Movement of the vortex caused large positively correlated fluctuations of temperature and all the stratospheric trace gases, making difficult the separation of temporal trends from the effects of spatial inhomogeneity. But, between the two periods when the centre of the vortex was near McMurdo (15–22 September and 15–23 October) even though the temperature increased at all levels there was very little change in the column abundances of HNO_3 which suggests that if this was indeed the same airmass, little HNO_3 was frozen out.

The chlorine species, on the other hand, show large increases between these two periods, suggesting that during September, a major fraction of the total stratospheric chlorine burden is either frozen out or is present in some molecular form other than HCl or $ClONO_2$. The chemical partitioning between HCl and $ClONO_2$ is also highly abnormal during September, both inside and near the edge of the vortex. While this is not proof of a cause and effect relationship between halogenated source gases and the springtime ozone depletion, it is entirely consistent with such hypotheses.

We thank our colleagues G. Mohler, R. H. Norton, R. J. Wilson, S. R. Paradise, D. C. Petterson, S. H. Nolte and J. Raney for their considerable efforts in the design and operation of the instrument, and for help with the reduction and analysis of the spectra. We are grateful for the assistance we received from the staff of the Polar Programs Division of the NSF and, in particular, the courtesy and cooperation extended to us by the ITT/ANS and US Navy personnel at McMurdo. This research was performed at the Jet Propulsion Laboratory, California Institute of Technology, under contract with NASA. The expedition to Antarctica was funded jointly by NASA and the NSF.

Received 29 June; accepted 12 August 1987.

1. Stolarski, R. S., Krueger, A. J., Newman, P. A. & Alpert, J. C. *Nature* **322**, 808–811 (1986).
2. Krueger, A. J., Schoeberl, M. R. & Stolarski, R. S. *Geophys. Res. Lett.* **14**, 5 (1987).
3. Farman, J. C., Gardiner, B. G. & Shanklin, J. D. *Nature* **315**, 207–210 (1985).
4. Hoffman, D. J., Harder, J. W., Rolf, G. R. & Rosen, J. M. *Nature* (in the press).
5. Brown, L. R., Farmer, C. B., Rinsland, C. P. & Toth, R. A. *Appl. Opt.* (in the press).
6. Ballard, J., Johnston, W. C., Gunson, M. R. & Wessell, P. T. *Geophys. Res. Lett.* (submitted).
7. Davidson, J. A., Cantrell, C. A., Shetter, C. A., McDaniel, A. H. & Calvert, J. G. *J. geophys. Res.* (in the press).
8. Callis, L. B. & Natarajan, M. *J. geophys. Res.* **91**, 771 (1986).
9. *WMO/NASA Atmospheric Ozone 1985: A Statement of our Understanding of the Processes Controlling its Present Distribution and Change, World Meteorological Organization Global Ozone Research and Monitoring Project, Report No. 16 1986* (1986).
10. Russell, J. M. *et al. J. geophys. Res.* (submitted).
11. Mount, G., Sanders, R., Schmelrekopf, A. & Solomon, S. *J. geophys. Res.* (in the press).
12. Raper, O. F., Farmer, C. B., Zander, R. & Park, J. H. *J. geophys. Res.* (in the press).
13. Zander, R., Rinsland, C. P., Farmer, C. B., Brown, L. R. & Norton, R. H. *Geophys. Res. Lett.* **13**, 457–760 (1986).
14. Farmer, C. B. & Raper, O. F. *Geophys. Res. Lett.* **4**, 527–529 (1977).
15. Farmer, C. B. & Raper, O. F. *NASA Conf. Proc. Spacelab 3 Mission Rev. CP-2429*, 42–62 (NASA, Washington DC, 1986).